Supplementary information files for Reversible P–P bond cleavage at an iridium(iii) metal centre

Electronic supplementary information

Reversible P–P bond cleavage at an iridium(III) metal centre

Simon J. Coles,[a] Peter N. Horton,[a] Patrick Kimber,[b] Wim T. Klooster,[a] Pingchuan Liu,[b]

Felix Plasser,[b] Martin B. Smith,*[b] and Graham J. Tizzard[a]

---

[a] *UK National Crystallography Service, School of Chemistry, University of Southampton, Southampton, SO17 1BJ.*

[b] *Department of Chemistry, Loughborough University, Loughborough, Leics, LE11 3TU, UK*.

E-mail: m.b.smith@lboro.ac.uk.

Experimental section

General methods and materials

The synthesis of ligand **P–P(OMe)** was carried out in air and was reproduceable. Tetrahydroxymethylphosphonium chloride (THPC) was provided as a kind donation from Solvay. All co-ordination reactions were carried out in air, using reagent grade quality solvents. The compounds $[IrCl(\mu\text{-}Cl)(\eta^5\text{-}C_5Me_5)]_2$ and AuCl(tht) (tht = tetrahydrothiophene) were both prepared according to known procedures.[1,2] All other chemicals were obtained from commercial sources and used directly without further purification.

Infrared spectra were recorded as KBr pellets on a Perkin-Elmer Spectrum 100S (4000–250 cm^{-1} range) Fourier-Transform spectrometer. ^1H NMR (400 or 500 MHz) and $^{13}C\{^1H\}$ NMR (101 or 126 MHz) spectra were recorded on a Jeol-ECS-400 FT or Jeol-ECZ-R-500 spectrometer with chemical shifts (δ) in ppm to high frequency of $Si(CH_3)_4$ and coupling constants (*J*) in Hz. $^{31}P\{^1H\}$ NMR (162 or 202 MHz) spectra were recorded on a Jeol-ECS-400 FT or Jeol-ECZ-R-500 spectrometer with chemical shifts (δ) in ppm to high frequency of 85% H_3PO_4. NMR spectra were measured in $CDCl_3$ at 298 K. Elemental analyses (Perkin-Elmer 2400 CHN or Exeter Analytical, Inc. CE-440 Elemental Analyzers) were performed by the Loughborough University Analytical Service within the Department of Chemistry.

Preparation of P–P(OMe). 4-methoxyaniline (6.15 g, 0.050 mmol) was dissolved in MeOH (1 L). Under vigorous stirring solid THPC (2.35 g, 0.0125 mol) was added at room temperature. After stirring for 60 h, an off-white solid **P–P(OMe)** was filtered from the black solution and dried *in vacuo*. Yield: 0.983 g, 44%. Selected data for **P–P(OMe)**: ^1H (400 MHz, $CDCl_3$, *δ*, *J* in Hz) 6.86 (4H, dd, $^3J_{HH}$ 10.4, arom. C*H*), 6.78 (4H, t, $^3J_{HH}$ 9.2, arom.

C*H*), 3.76 (6H, s, CH_3), 3.54–3.46 (8H, m, PCH_2N). $^{13}C\{^1H\}$ NMR (101 MHz, $CDCl_3$, δ, *J* in Hz) 153.9, 143.8, 114.6, 55.7 (*C*H_3), 54.6 (J_{PC} 27, P*C*H_2N). $^{31}P\{^1H\}$ NMR (162 MHz, $CDCl_3$, δ) –34.7. IR (KBr, *v* cm^{-1}): 3468, 2808, 1295, 1237. Anal. Calcd for $C_{18}H_{22}N_2O_2P_2$ (%): C, 60.00; H, 6.17; N, 7.78. Found: C, 60.07; H, 6.09; N, 7.81. Crystals of **P–P(OMe)** were grown by slow diffusion of diethyl ether/hexanes into a $CDCl_3$ solution.

Preparation of 1. An orange CH_2Cl_2 (10 mL) solution of $[IrCl(\mu\text{-}Cl)(\eta^5\text{-}C_5Me_5)]_2$ (0.052 g, 0.065 mmol) and **P–P(OMe)** (0.047 g, 0.13 mmol) was stirred for 10 min. The volume of solvent was reduced to *ca.* 1–2 mL under reduced pressure and diethyl ether (20 mL) added to precipitate **1** as a yellow solid. Yield: 0.088 g, 88%. Selected data for **1**: ^1H (400 MHz, $CDCl_3$, δ, *J* in Hz) 6.87 (4H, d, $^3J_{HH}$ 8.8, arom. C*H*), 6.77 (4H, d, $^3J_{HH}$ 6.8, arom. C*H*), 4.10 (1H, dt, 12.4, 1.9, CH_2), 3.96 (1H, ddd, 12.4, 6.2, 2.6, CH_2), 3.77–3.67 (8H, m, CH_2 and CH_3), 1.74 (15H, d, $^4J_{PH}$ 2.7, Cp*). $^{13}C\{^1H\}$ NMR (101 MHz, $CDCl_3$, δ, *J* in Hz) 154.2, 143.0, 118.8, 114.8, 92.5, 55.7 (*C*H_3), 54.5 (J_{PC} 28, P*C*H_2N), 52.1 (J_{PC} 24, P*C*H_2N), 9.0. $^{31}P\{^1H\}$ NMR (162 MHz, $CDCl_3$, δ) 15.8 (d, J_{PP} 230 Hz, IrP), –56.3 (free P) ppm. Anal. Calcd for $C_{28}H_{37}N_2O_2P_2IrCl_2{\cdot}CH_2Cl_2$ (%): C, 44.33; H, 4.93; N, 3.69. Found: C, 43.83; H, 4.73; N, 3.63. Crystals of **1** were grown by vapour diffusion of diethyl ether into a $CDCl_3$ solution.

Preparation of 1`. To an orange CH_2Cl_2 (20 mL) solution of $[IrCl(\mu\text{-}Cl)(\eta^5\text{-}C_5Me_5)]_2$ (0.100 g, 1.26 mmol) was added **P–P(OMe)** (0.046 g, 1.28 mmol). The solution was stirred for 15 min, the volume of solvent reduced to *ca.* 1–2 mL under reduced pressure and diethyl ether (30 mL) to precipitate **1`** as an orange solid. Yield: 0.127 g, 87%. Selected data for **1`**: ^1H (500 MHz, $CDCl_3$, δ, *J* in Hz) 6.88 (4H, d, $^3J_{HH}$ 10, arom. C*H*), 6.78 (4H, d, $^3J_{HH}$ 10, arom.

C*H*), 4.32 (8H, br, CH_2), 3.75 (6H, s, CH_3), 1.77 (15H, s, Cp*). $^{13}C\{^1H\}$ NMR (101 MHz, $CDCl_3$, δ) 154.3, 142.4, 118.4, 114.8, 93.7, 55.7 (*C*H_3), 54.7 (P*C*H_2N), 9.5. $^{31}P\{^1H\}$ NMR (202 MHz, $CDCl_3$, δ) −7.2 ppm. Anal. Calcd for $C_{38}H_{52}N_2O_2P_2Ir_2Cl_4 \cdot 0.5CH_2Cl_2$ (%): C, 38.55; H, 4.46; N, 2.34. Found: C, 38.28; H, 4.31; N, 2.37.

Preparation of 2. A yellow CH_2Cl_2 (20 mL) solution of $[IrCl(\mu\text{-}Cl)(\eta^5\text{-}C_5Me_5)]_2$ (0.102 g, 0.128 mmol) and **P–P(OMe)** (0.094 g, 0.261 mmol) was stirred for 5 min. AuCl(tht) (0.082 g, 0.256 mmol) was added as a solid and the resulting solution stirred for a further 10 mins. The volume of solvent was reduced to *ca.* 1–2 mL under reduced pressure and diethyl ether (25 mL) added to precipitate **2** as a pale yellow solid. Yield: 0.210 g, 83%. Selected data for **2**: ^1H (500 MHz, $CDCl_3$, δ, *J* in Hz) 6.99 (2H, d, $^3J_{HH}$ 6.4, arom. C*H*), 6.94 (2H, d, $^3J_{HH}$ 6.3, arom. C*H*), 6.87 (2H, d, $^3J_{HH}$ 6.4, arom. C*H*), 6.82 (2H, d, $^3J_{HH}$ 6.4, arom. C*H*), 4.83 (1H, t, $^2J_{HH}$ 11.5, CH_2), 4.23 (2H, dd, $^2J_{HH}$ 14.0, 6.8, CH_2), 3.97 (1H, d, $^2J_{HH}$ 13.9 CH_2), 3.87, 3.78 (3H, s, CH_3), 3.75 (3H, s, CH_3), 3.48–3.45 (H, dd, CH_2), 1.95 (15H, s, Cp*). $^{13}C\{^1H\}$ NMR (101 MHz, $CDCl_3$, δ, *J* in Hz) 155.7, 155.0, 146.6, 145.0, 121.0, 119.1, 115.0, 99.8, 55.7 (*C*H_3), 54.1 (J_{PC} 48, P*C*H_2N), 53.2 (J_{PC} 43, P*C*H_2N), 48.5 (J_{PC} 59, P*C*H_2N), 9.5. $^{31}P\{^1H\}$ NMR (202 MHz, $CDCl_3$, δ) 66.9 (d, J_{PP} 53.5 Hz, AuP), –38.1 (IrP) ppm. IR (KBr, ν cm^{-1}): 314 (AuCl). Anal. Calcd for $C_{28}H_{37}N_2O_2P_2AuIrCl_3$ (%): C, 33.93; H, 3.77; N, 2.83. Found: C, 33.79; H, 3.76; N, 3.47. Crystals of **2** were grown by vapour diffusion of diethyl ether into a $CDCl_3$ solution.

Preparation of 3. A $CDCl_3$ (0.7 mL) solution of **2** (0.0144 g, 0.015 mmol) was heated at 50 °C for approx. 4 d. After cooling, significant decomposition material was removed by filtration through a small plug and the resulting solution layered with hexanes. Yield: 0.003 g, 21%. Selected data for **3**: ^1H (400 MHz, $CDCl_3$, δ, *J* in Hz) 6.99 (1H, d, $^3J_{HH}$ 8.7, arom. C*H*),

6.87 (2H, d, $^{3}J_{HH}$ 9.3, arom. C*H*), 6.77 (3H, m, arom. C*H*), 5.78 (1H, t, $^{2}J_{HH}$ 2.4, arom. C*H*), 5.41 (1H, t, $^{2}J_{HH}$ 13.4, CH_2), 5.34 (1H, dd, $^{2}J_{HH}$ 12.4, CH_2), 4.35 (1H, dd, $^{2}J_{HH}$ 14.6, 9.1, CH_2), 4.18 (1H, ddd, $^{2}J_{HH}$ 13.9, 7.6, 1.6, CH_2), 4.07 (1H, d, $^{2}J_{HH}$ 14.8, CH_2), 3.77 (3H, s, CH_3), 3.40 (3H, s, CH_3), 2.67 (1H, d, $^{2}J_{HH}$ 13.8, CH_2), 1.90 (15H, s, Cp*). $^{13}C\{^{1}H\}$ NMR (126 MHz, $CDCl_3$, δ, *J* in Hz) 157.2, 154.9, 142.3, 127.1, 126.6, 120.4, 116.7, 115.0, 112.8, 99.6, 69.0, 68.5, 55.6 (*C*H_3), 55.3 (*C*H_3), 51.8 (J_{PC} 18, P*C*H_2N), 48.0, 41.6 (J_{PC} 34, P*C*H_2N), 9.4. $^{31}P\{^{1}H\}$ NMR (162 MHz, $CDCl_3$, δ) 50.5 (d, J_{PP} 55.7 Hz, AuP), −30.2 (IrP) ppm. IR (KBr, *v* cm^{-1}): 319 (AuCl). Anal. Calcd for $C_{28}H_{35}N_2O_2P_2AuIrCl_3 \cdot CDCl_3$ (%): C, 31.42; H, 3.28; N, 2.53. Found: C, 31.64; H, 2.92; N, 2.48. Crystals of **3** were grown by slow diffusion of hexanes into a $CDCl_3$ solution.

NMR data

Figure S1 ^{1}H NMR spectrum of compound **P–P(OMe)** (recorded in $CDCl_3$).

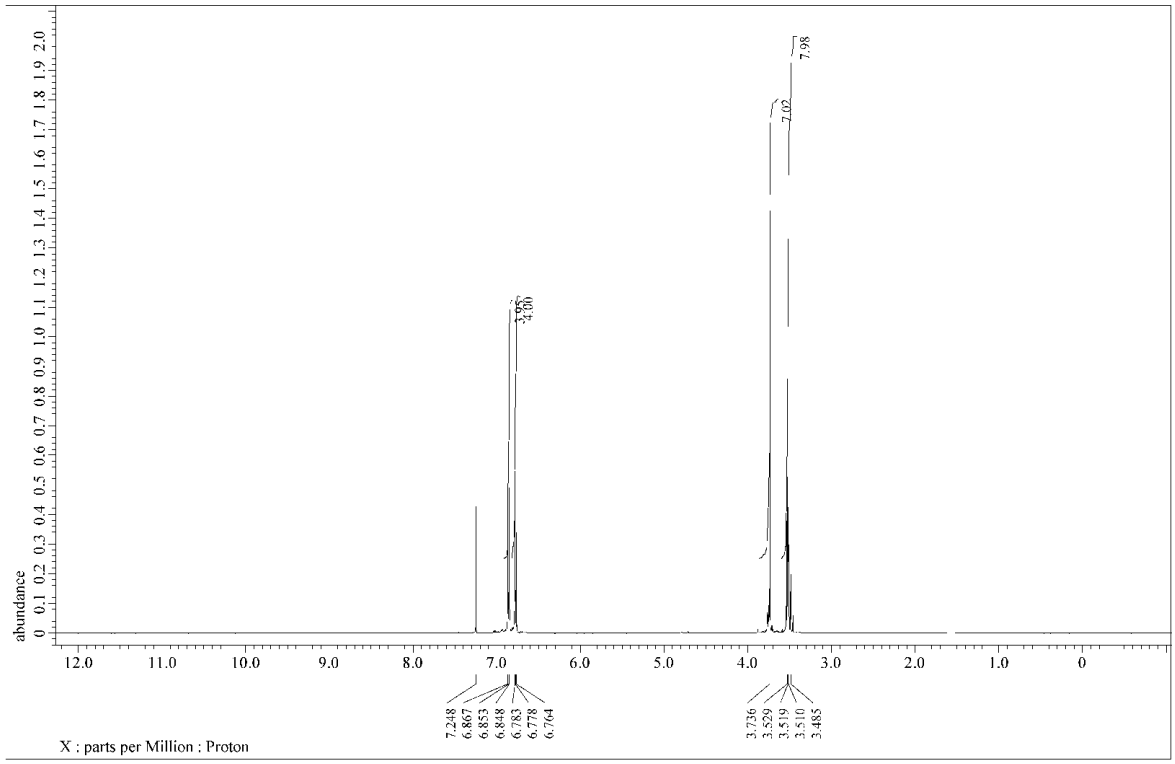

Figure S2 $^{13}C\{^{1}H\}$ NMR spectrum of compound **P–P(OMe)** (recorded in $CDCl_3$).

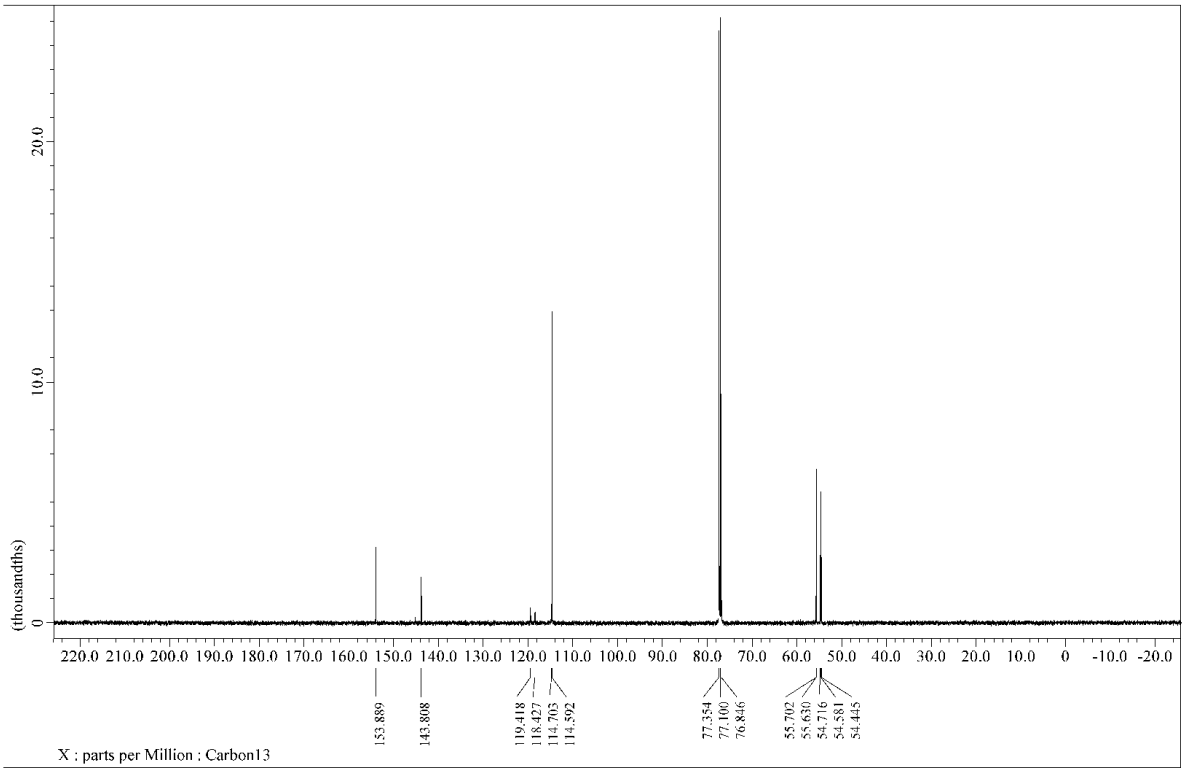

Figure S3 $^{31}P\{^{1}H\}$ NMR spectrum of compound **P–P(OMe)** (recorded in $CDCl_3$).

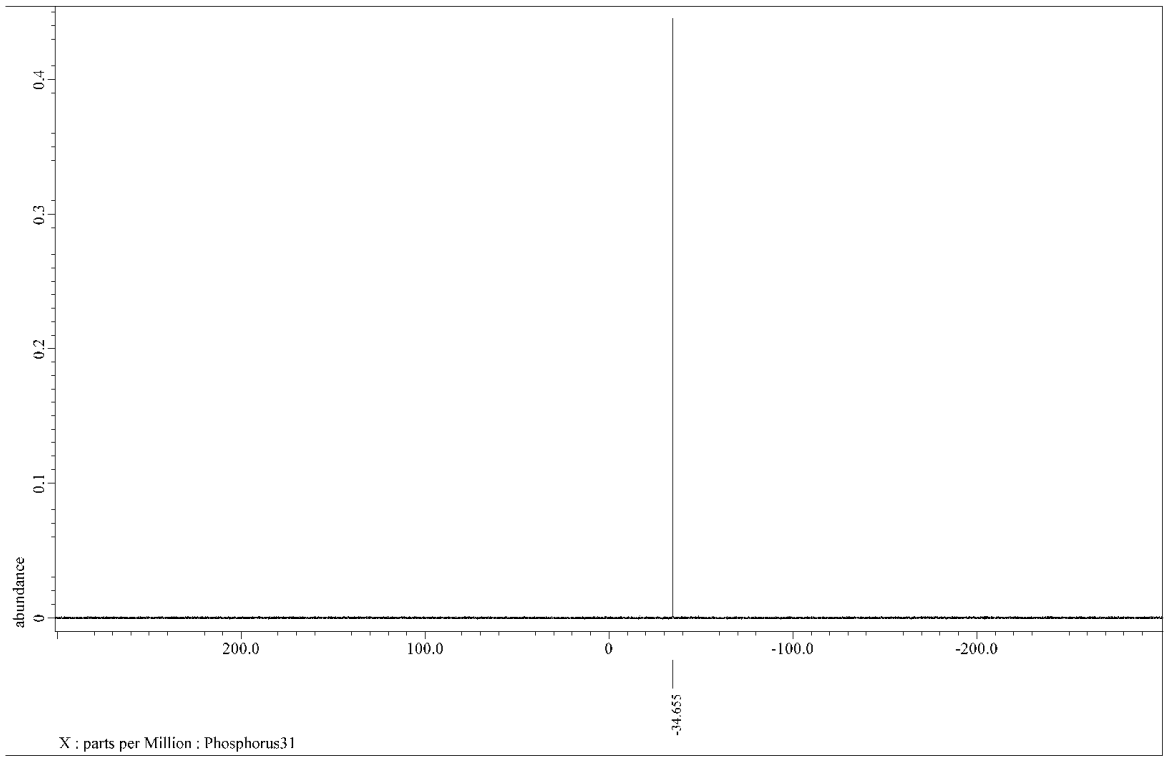

Figure S4 ^{1}H NMR spectrum of compound **1** (recorded in $CDCl_3$).

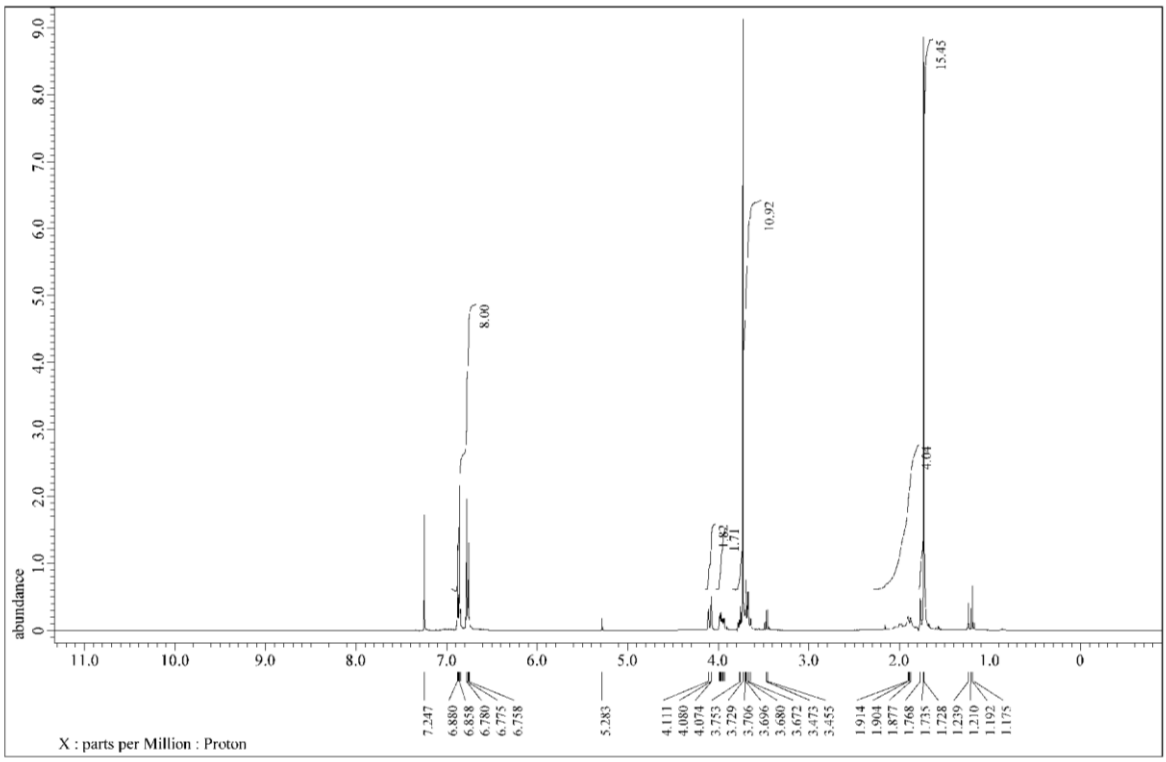

Figure S5 $^{13}C\{^{1}H\}$ NMR spectrum of compound **1** (recorded in $CDCl_3$).

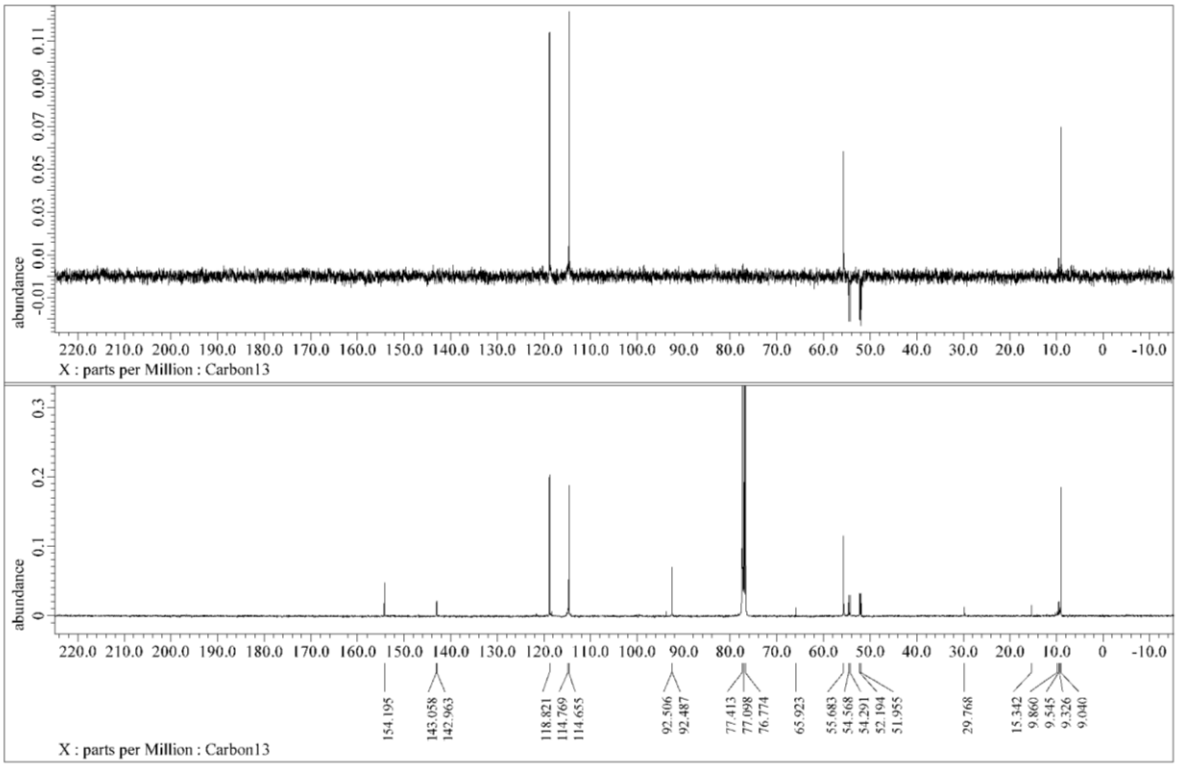

Figure S6 $^{31}P\{^{1}H\}$ NMR spectrum of compound **1** (recorded in $CDCl_3$).

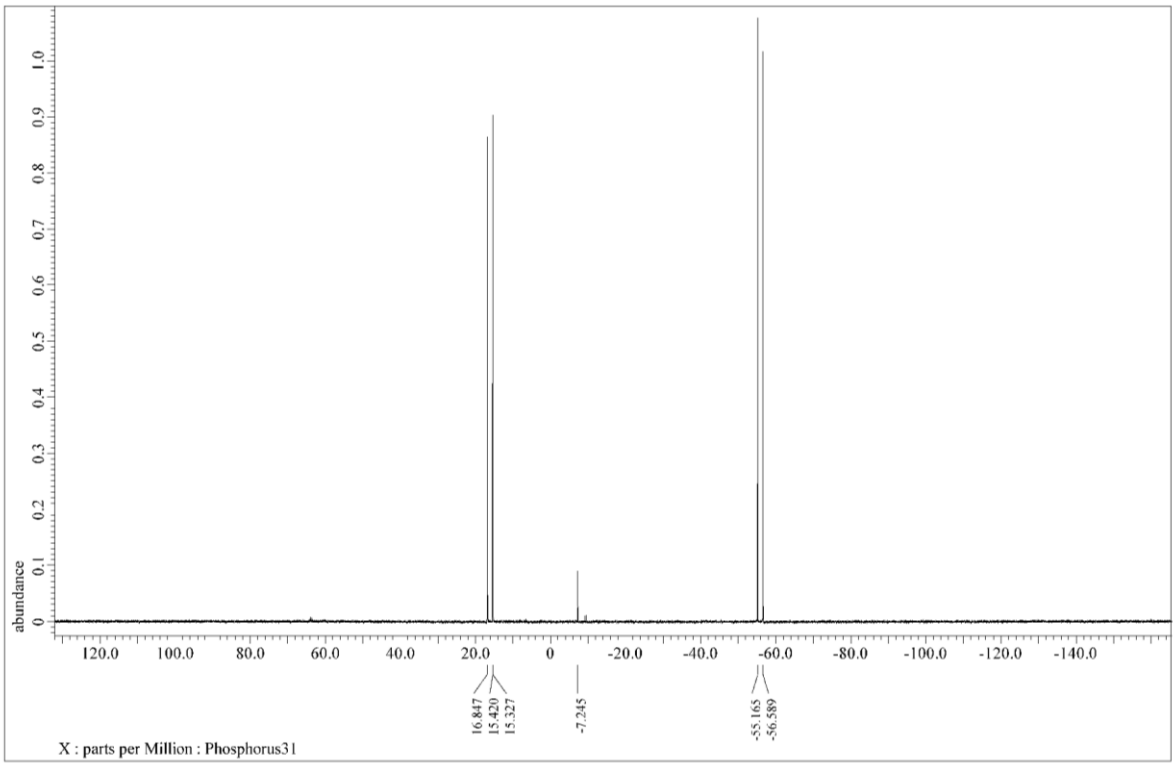

Figure S7 ^{1}H NMR spectrum of compound **1`** (recorded in $CDCl_3$).

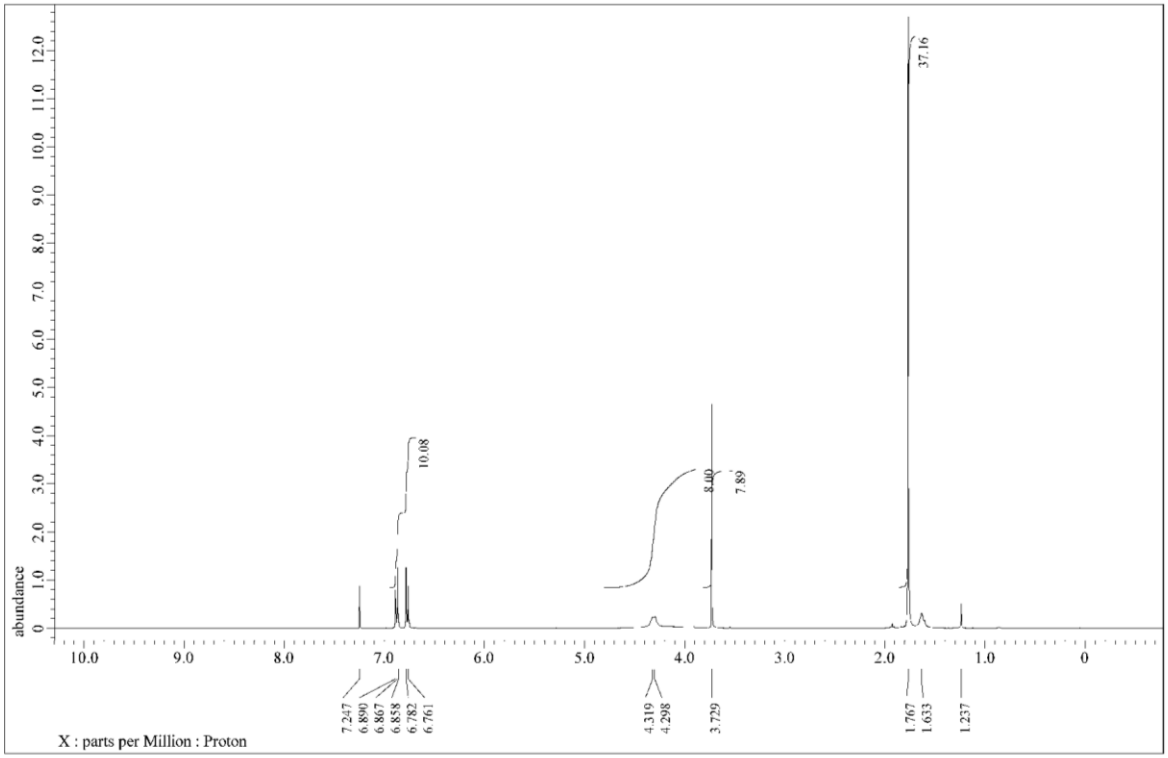

Figure S8 $^{13}C\{^{1}H\}$ NMR spectrum of compound **1`** (recorded in $CDCl_3$).

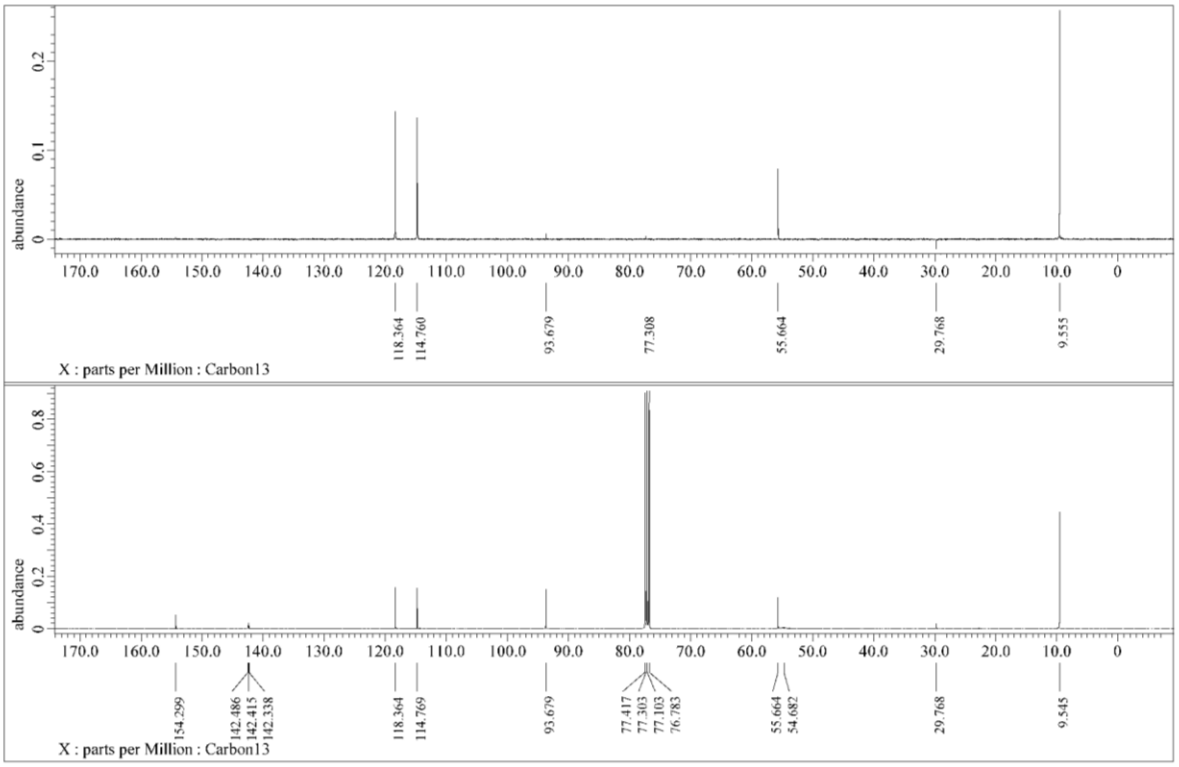

Figure S9 $^{31}P\{^{1}H\}$ NMR spectrum of compound **1`** (recorded in $CDCl_3$).

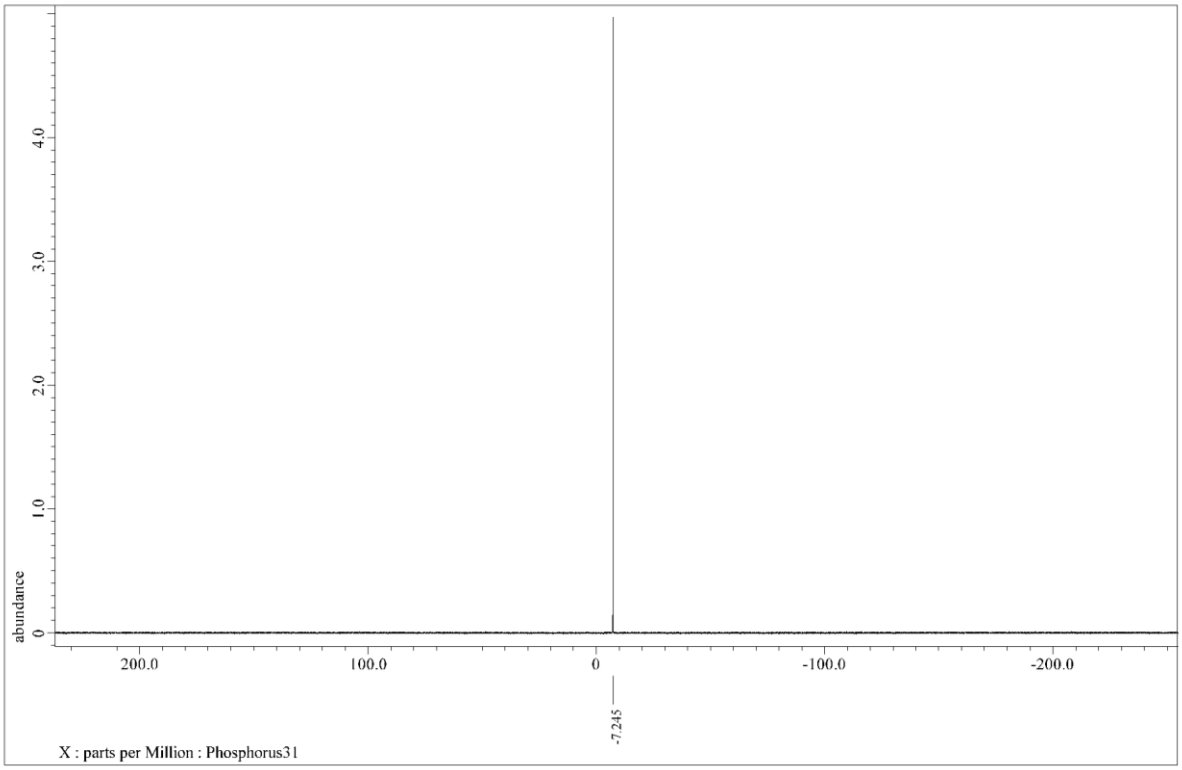

Figure S10 ^{1}H NMR spectrum of compound **2** (recorded in $CDCl_3$).

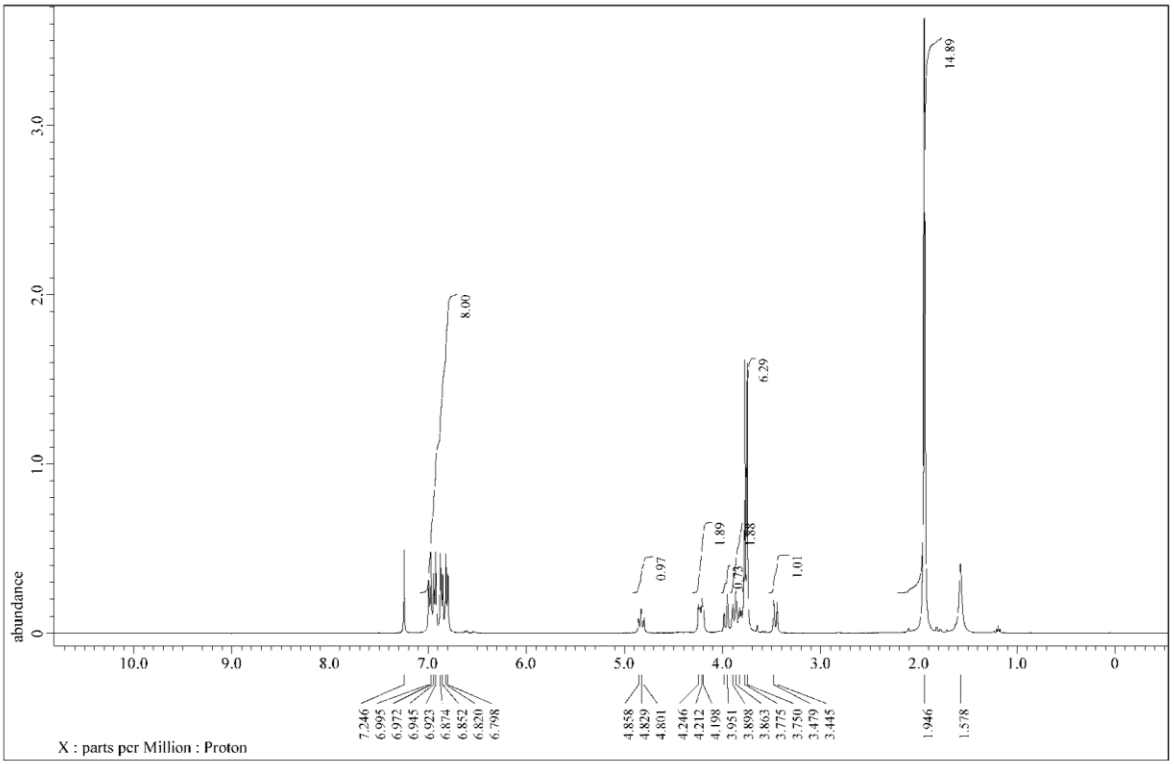

Figure S11 $^{13}C\{^{1}H\}$ NMR spectrum of compound **2** (recorded in $CDCl_3$).

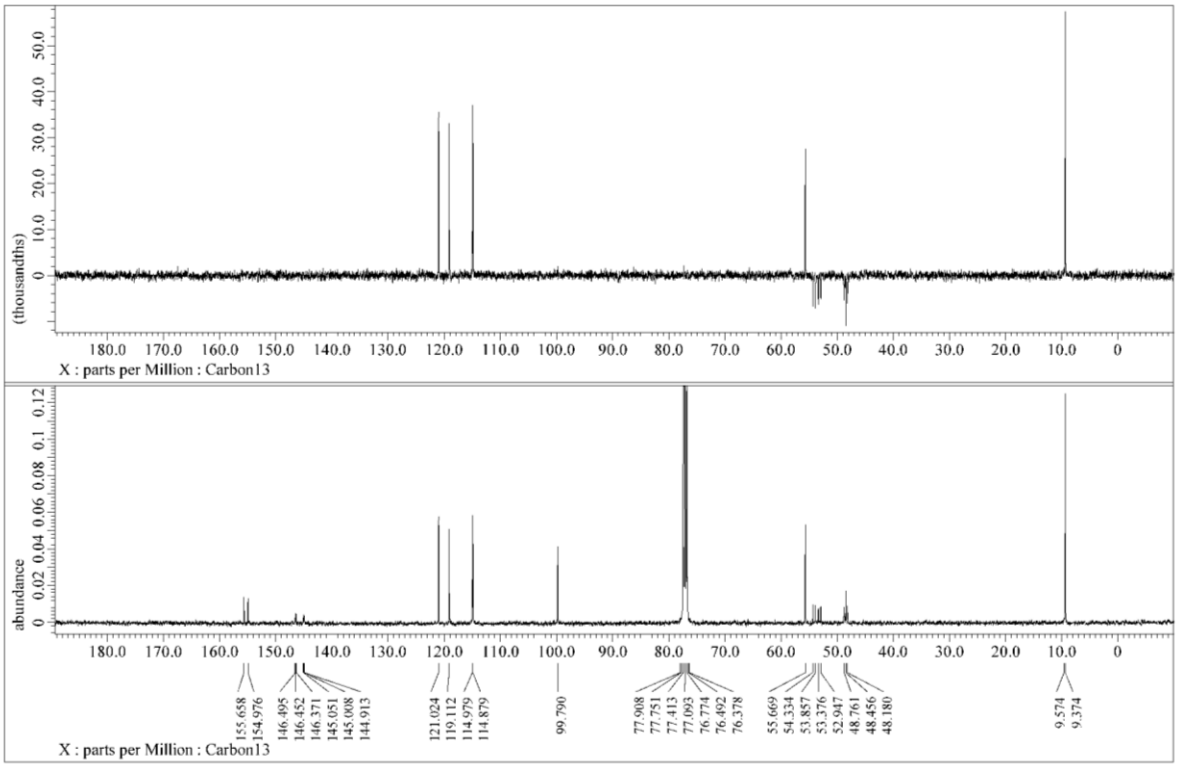

Figure S12 $^{31}P\{^{1}H\}$ NMR spectrum of compound **2** (recorded in $CDCl_3$).

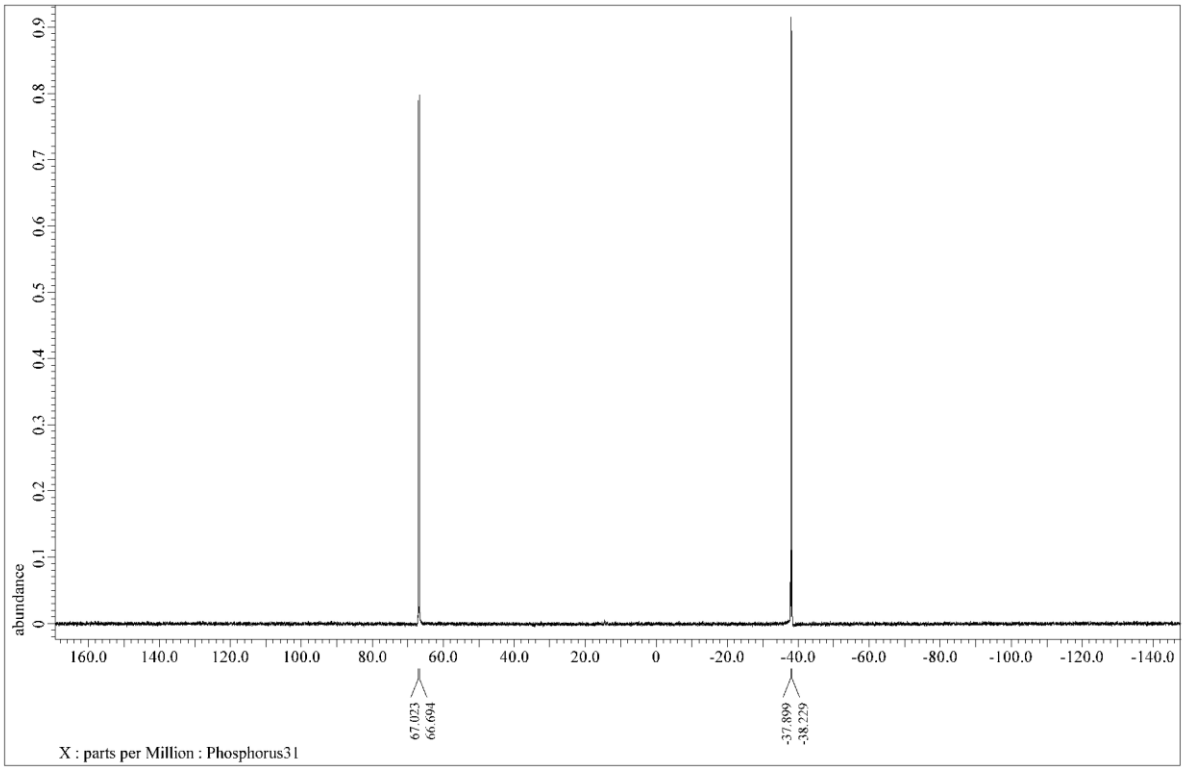

Figure S13 ^{1}H NMR spectrum of compound **3** (recorded in $CDCl_3$).

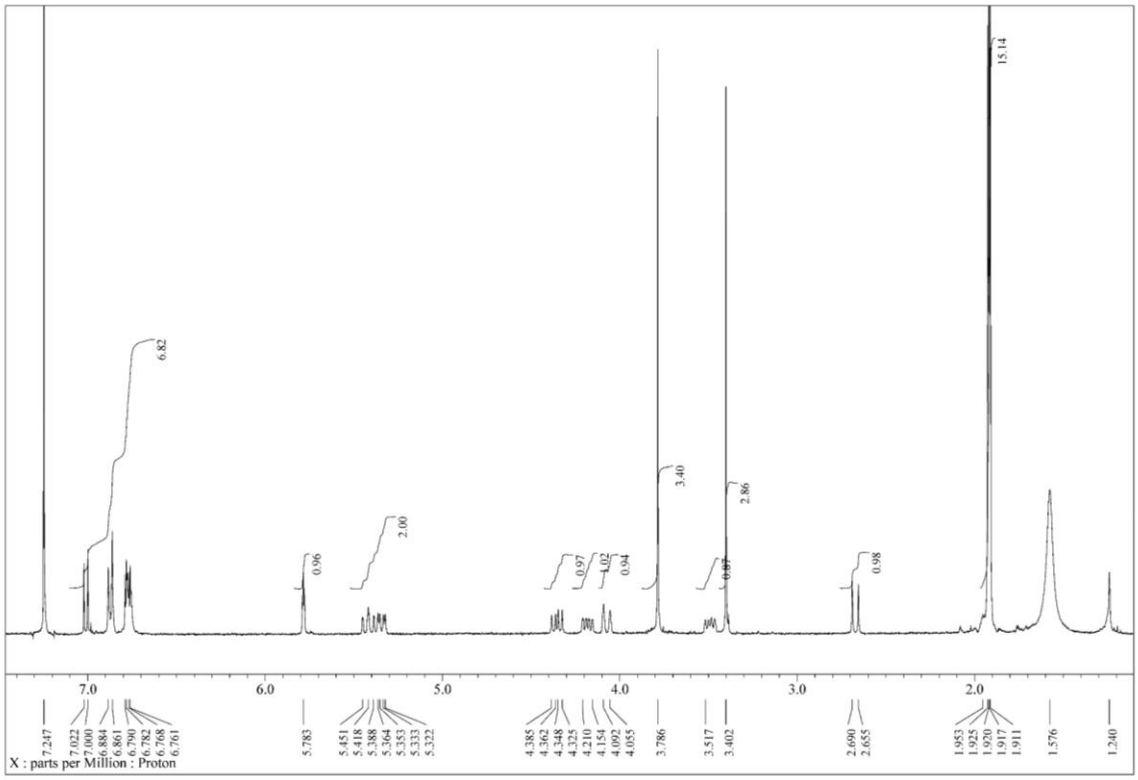

Figure S14 $^{13}C\{^{1}H\}$ NMR spectrum of compound **3** (recorded in $CDCl_3$).

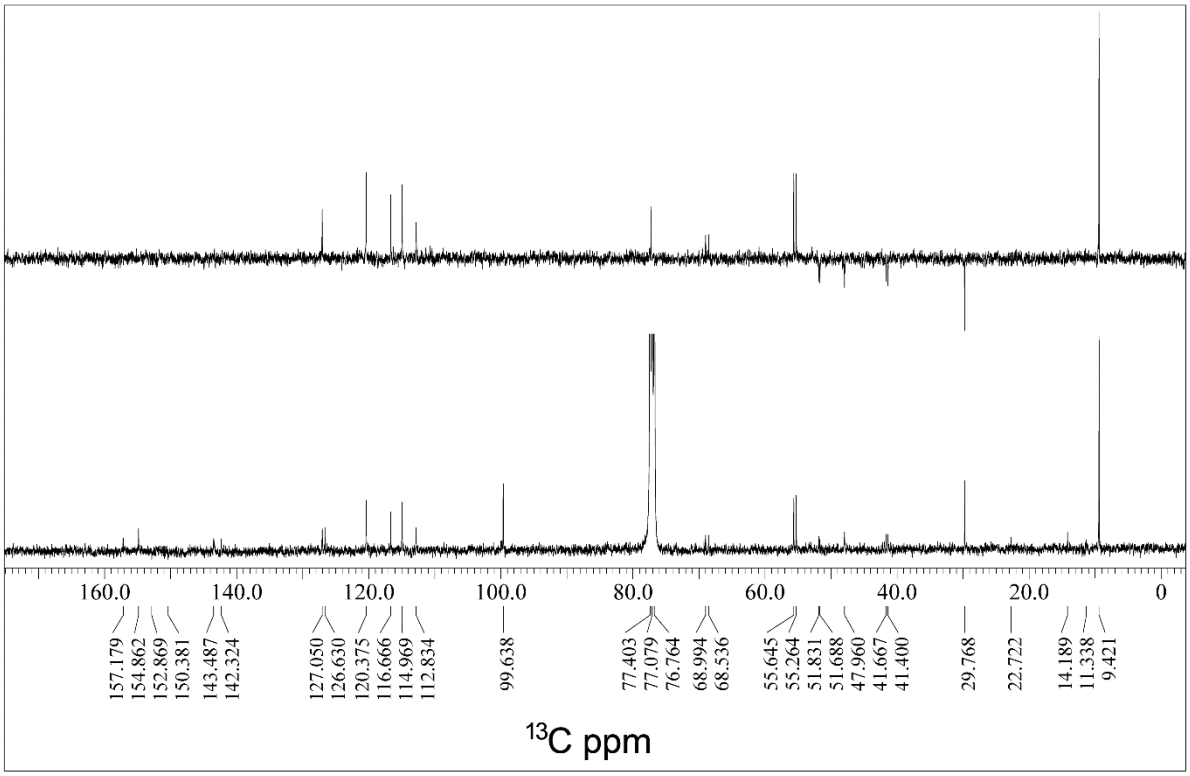

Figure S15 $^{31}P\{^{1}H\}$ NMR spectrum of compound **3** (recorded in $CDCl_3$).

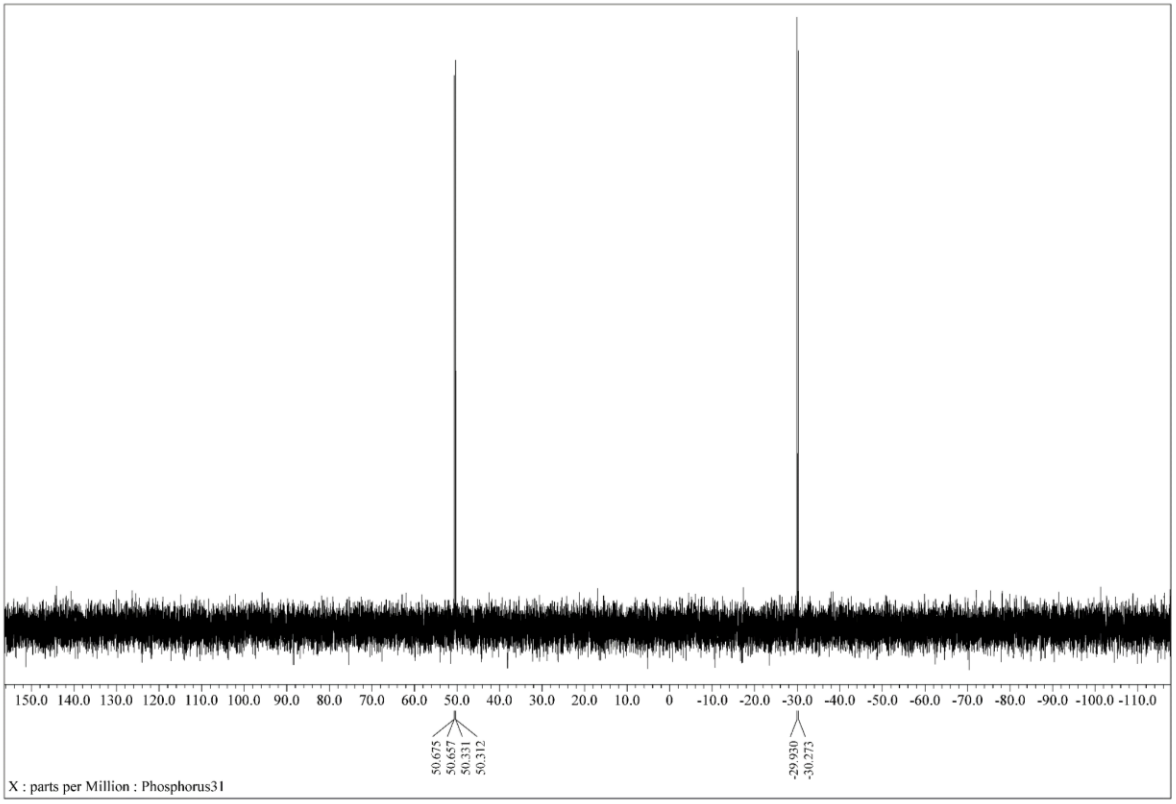

Figure S16 $^{31}P\{^{1}H\}$ NMR study of **3** and PPh_3 (1 eq.) (recorded in $CDCl_3$).

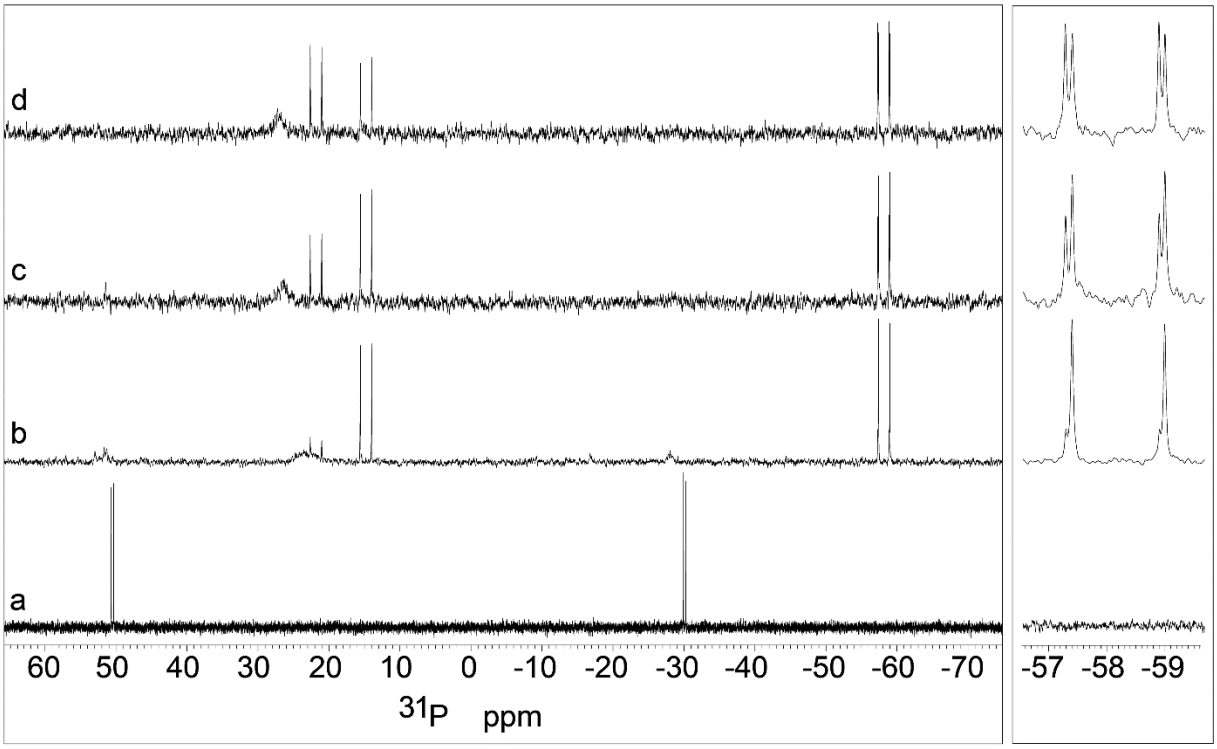

X-ray Crystallography Experimental

All single crystal X-ray crystallographic studies were carried out at the UK National Crystallography Service at the University of Southampton. Suitable crystals of **P–P(OMe)** were obtained by slow diffusion of diethylether and hexanes into a CH_2Cl_2 solution whereas for compound **3·CDCl₃**, crystals were obtained by slow diffusion of hexanes into a $CDCl_3$ solution. Suitable crystals of **1** and **2·CDCl₃** were obtained by vapour diffusion of diethyl ether into $CDCl_3$ solutions.

Experimental for P–P(OMe). A suitable colourless block-shaped crystal of **P–P(OMe)** (0.21×0.15×0.07 mm^3) was selected and mounted on a MITEGEN holder in perfluoroether oil on a Rigaku FRE+ diffractometer equipped with Arc)Sec VHF Varimax confocal mirrors and an AFC12 goniometer and HyPix 6000HE detector.[3] The crystal was kept at a steady T = 100(2) K during data collection. The structure was solved with the ShelXT 2014/5 structure solution program[4] using the Intrinsic Phasing solution method and by using Olex2[5] as the graphical interface. The model was refined with version 2014/7 of ShelXL[6] using Least Squares minimisation. All non-hydrogen atoms were refined anisotropically. Hydrogen atom positions were calculated geometrically and refined using the riding model.

Crystal Data for P–P(OMe). $C_{18}H_{22}N_2O_2P_2$, M_r = 360.31, orthorhombic, $P2_12_12$ (No. 18), a = 26.9909(4) Å, b = 6.1009(1) Å, c = 5.1027(1) Å, $\alpha = \beta = \gamma = 90^\circ$, V = 840.26(2) $Å^3$, T = 100(2) K, Z = 2, Z' = 0.5, $\mu(MoK_a)$ = 0.273 mm^{-1}, 38376 reflections measured, 1936 unique (R_{int} = 0.0292) which were used in all calculations. The final wR_2 was 0.0545 (all data) and R_1 was 0.0203 (I > 2(I)).

Experimental for 1. A suitable yellow needle-shaped crystal of **1** (0.60×0.06×0.03 mm^3) was selected and mounted on a MITEGEN holder in perfluoroether oil on a Rigaku FRE+ diffractometer equipped with Arc)Sec VHF Varimax confocal mirrors and an AFC12 goniometer and HyPix 6000HE detector.[3] The crystal was kept at a steady T = 100(2) K during data collection. The structure was solved with the ShelXT 2014/5 structure solution program[4] using the Intrinsic Phasing solution method and by using Olex2[5] as the graphical interface. The model was refined with version 2014/7 of ShelXL[6] using Least Squares minimisation. All non-hydrogen atoms were refined anisotropically. Hydrogen atom positions were calculated geometrically and refined using the riding model.

Crystal Data for 1. $C_{28}H_{37}Cl_2IrN_2O_2P_2$, M_r = 758.63, monoclinic, *Cc* (No. 9), a = 14.2647(3) Å, b = 24.6280(4) Å, c = 8.18186(15) Å, β = 98.2803(18)°, α = γ = 90°, V = 2844.42(9) $Å^3$, T = 100(2) K, Z = 4, Z' = 1, μ(MoK_a) = 5.024 mm^{-1}, 31747 reflections measured, 6469 unique (R_{int} = 0.0289) which were used in all calculations. The final wR_2 was 0.0589 (all data) and R_1 was 0.0232 (I > 2(I)).

Experimental for 2·CDCl₃. A suitable yellow block-shaped crystal of **2·CDCl₃** (0.18×0.011×0.005 mm^3) was selected and mounted on a MITEGEN holder in perfluoroether oil on a Rigaku FRE+ diffractometer equipped with Arc)Sec VHF Varimax confocal mirrors and an AFC12 goniometer and HyPix 6000HE detector.[3] The crystal was kept at a steady T = 100(2) K during data collection. The structure was solved with the ShelXT 2018/2 structure solution program[4] using the Intrinsic Phasing solution method and by using Olex2[5] as the graphical interface. The model was refined with version 2018/3 of ShelXL[6] using Least Squares minimisation. All non-hydrogen atoms were refined anisotropically. Hydrogen atom positions were calculated geometrically and refined using the riding model. Thermal

restraints were applied to one of the methoxy groups (O2, C18)

Crystal Data for 2·CDCl₃. $C_{57}H_{74}Au_2Cl_9DIr_2N_4O_4P_4$, M_r = 2102.47, orthorhombic, $P2_12_12_1$ (No. 19), a = 13.0610(1) Å, b = 20.2888(1) Å, c = 25.7121(2) Å, $\alpha = \beta = \gamma = 90^\circ$, V = 6813.50(8) Å^3, T = 100(2) K, Z = 4, Z' = 1, μ(MoK$_a$) = 8.680 mm^{-1}, 193070 reflections measured, 15614 unique (R_{int} = 0.0449) which were used in all calculations. The final wR_2 was 0.0428 (all data) and R_1 was 0.0164 (I > 2(I)).

Experimental for 3·CDCl₃. A suitable yellow block-shaped crystal of **3·CDCl₃** (0.160×0.031×0.013 mm^3) was selected and mounted on a MITEGEN holder in perfluoroether oil on a Rigaku FRE+ diffractometer equipped with Arc)Sec VHF Varimax confocal mirrors and an AFC12 goniometer and HyPix 6000HE detector.[3] The crystal was kept at a steady T = 100.00(10) K during data collection. The structure was solved with the ShelXT 2014/5 structure solution program[4] using the Intrinsic Phasing solution method and by using Olex2[5] as the graphical interface. The model was refined with version 2014/7 of ShelXL[6] using Least Squares minimisation. All non-hydrogen atoms were refined anisotropically. Hydrogen atom positions were calculated geometrically and refined using the riding model. The solvent $CDCl_3$ was disordered over two positions (~69:31). The disorder components were refined with thermal restraints and geometric equal distance restraints between equivalent pairs of atoms of each disorder component.

Crystal Data for 3·CDCl₃. $C_{29}H_{35}AuCl_6DIrN_2O_2P_2$, M_r = 1109.41, orthorhombic, $P2_12_12_1$ (No. 19), a = 13.6870(2) Å, b = 15.3847(3) Å, c = 16.7249(3) Å, $\alpha = \beta = \gamma = 90^\circ$, V = 3521.77(11) Å^3, T = 100(2) K, Z = 4, Z' = 1, μ(MoK$_a$) = 8.513 mm^{-1}, 46521 reflections measured, 8067 unique (R_{int} = 0.0441) which were used in all calculations. The final wR_2 was 0.0656 (all data) and R_1 was 0.0294 (I > 2(I)).

CCDC 2143419, 2143421, 2143424 and 2143445 contain the supplementary crystallographic data for this paper.

Natural bond orbital (NBO) computations

The natural bond orbitals (NBOs) were computed to gain additional insight into the bonding of the ligand to the Ir and Au atoms. These NBOs are shown below.

Figure S17 NBOs computed for the free ligand representing (a) the P–P bond, and (b, c) the lone pairs. Below each figure, the contribution to the NBO from each atom is presented as a percentage; major contributions from atomic orbital types for each atom are given as a ratio.

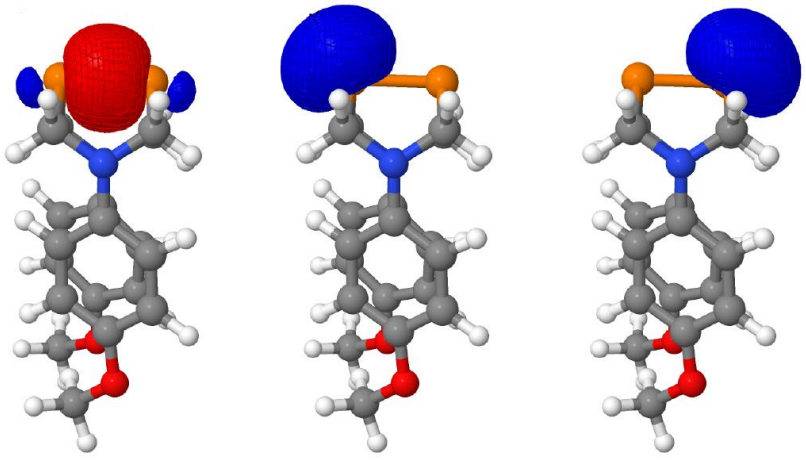

Figure S17 presents an analysis of the free ligand showing the NBOs representing the P–P bond and the lone pairs. Simple valence bond theory would suggest that the P atoms are sp^3 hybridised with the P–P bond and lone pairs in sp^3 orbitals (i.e. 0.25 s, 0.75 p). However, this simple picture does not apply as there is enhanced p-orbital character present in the P–P bond and enhanced s-character in the lone pairs.

Figure S18 NBOs computed for **1** representing (a) the Ir–P and (b) P–P bonds, and the (c) P(2) lone pair.

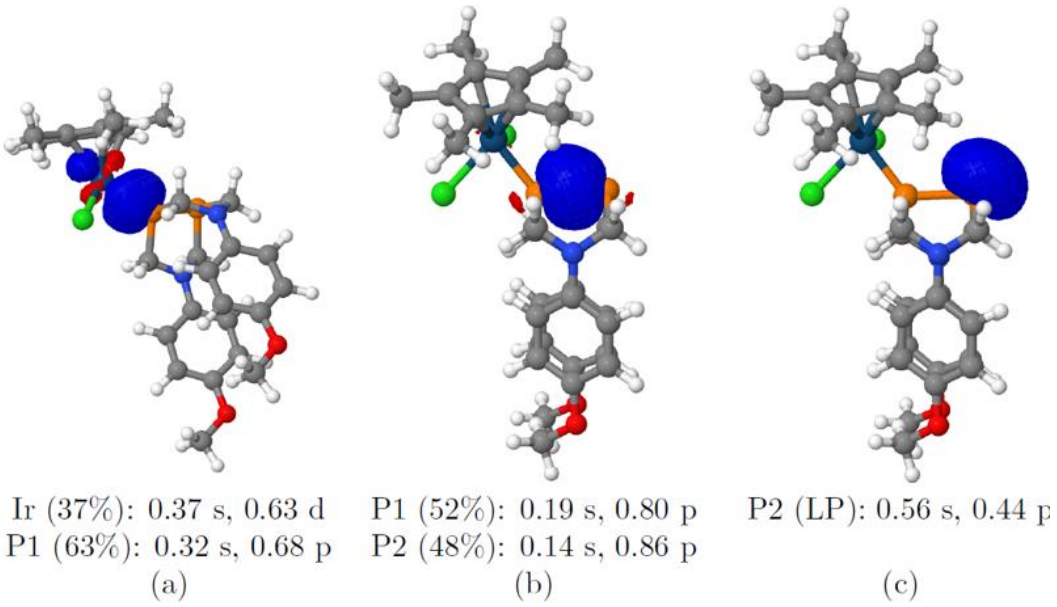

Figure S18 presents the NBOs computed for **1**. The Ir–P bonding orbital (Fig. S18, a) has notably reduced s-character when compared to the isolated lone pair (Fig. S18, b), effectively forming an sp^2 hybrid. The P–P bond has slightly reduced p-character.

Figure S19 NBOs computed for **2`** representing the (a) Ir–P and (b) P–P bonds, the (c) P(2) lone pair, (d) Au lone pair, and (e) Au lone pair.

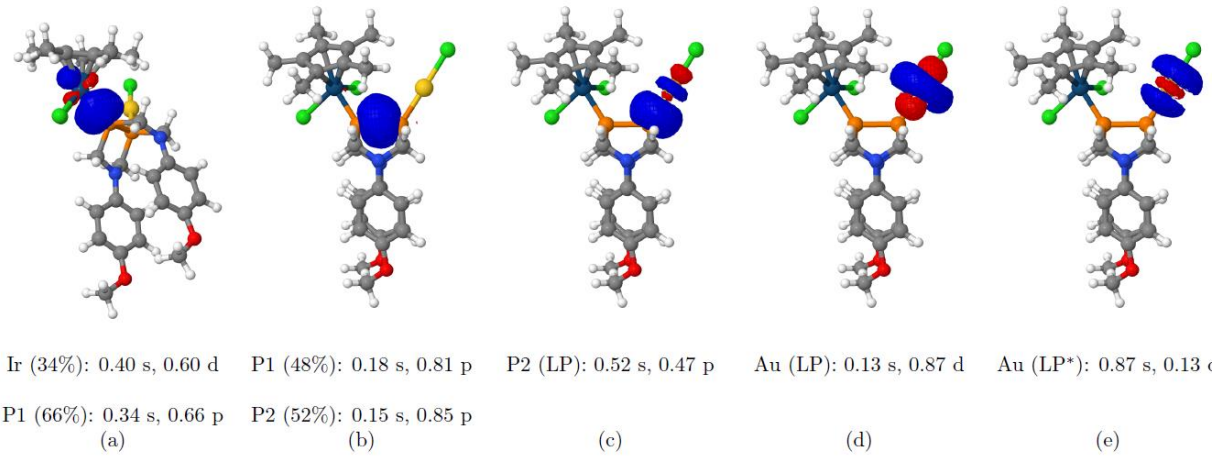

The NBOs of **2`** can be seen in Figure S19. The NBO analysis does not recognise a bonding interaction between P(2) and Au but finds an sp-hybridised lone pair on P(2) along with a d-type lone pair on Au. We interpret this finding in the sense that the sp-hybridised lone pair on P(2) is not able to form a bond with Au, and this incompatibility probably destabilises the **2`** structure.

Figure S20 NBOs computed for **2** representing the (a) Ir–P(1), (b) Ir–P(2), (c) P(2)–Au and (d) Au lone pair.

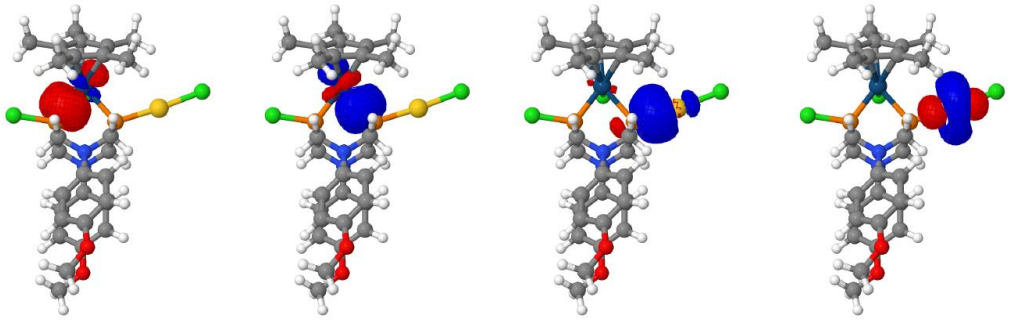

Finally, we consider the NBOs for the final product of the reaction, molecule **2**, in Figure S20. The description of the Ir–P bond does not change significantly compared to the previous two molecules retaining the sp^2 on P1 character. However, the picture is changed for P(2), which now forms an sp^3 hybrid able to bind with Au. Formation of the sp^3 hybrid is only possible after the P–P bond is broken as this bond required enhanced p-character. We interpret this change in hybridisation as a major contributor to the difference in stability between **2`** and **2**.

Computational details

Density Functional Theory calculations in this work were performed in Q-Chem 5.2.[7] All structures were optimised at the D3-TPSSh/def2-TZVP level of theory, using the def2-ECP

effective core potential.[8–10] The optimised geometries of the unobserved compound **2`** and compound **2** were used to perform a freezing string calculation to locate an approximate transition state.[11,12] The approximate transition state was optimised to a saddle point, confirmed *via* a vibrational analysis. Natural bond orbital analysis was carried out on the optimised structures.[13]

References

1. C. White, A. Yates and P. M. Maitlis, *Inorg. Synth.*, 1992, **29**, 228–234.
2. R. Uson, A. Laguna and M. Laguna, *Inorg. Synth.*, 1989, **26**, 85–91.
3. CrysAlisPro Software System, Rigaku Oxford Diffraction, 2020.
4. G. M. Sheldrick, ShelXT-Integrated space-group and crystal-structure determination, *Acta Cryst.*, 2015, **A71**, 3–8.
5. O. V. Dolomanov and L. J. Bourhis and R. J. Gildea and J. A. K. Howard and H. Puschmann, Olex2: A complete structure solution, refinement and analysis program, *J. Appl. Cryst.*, 2009, **42**, 339–341.
6. G. M. Sheldrick, Crystal structure refinement with ShelXL, *Acta Cryst.*, 2015, **C27**, 3–8.
7. Y. Shao, Z. Gan, E. Epifanovsky, A. T. Gilbert, M. Wormit, J. Kussmann, A. W. Lange, A. Behn, J. Deng, X. Feng, D. Ghosh, M. Goldey, P. R. Horn, L. D. Jacobson, I. Kaliman, R. Z. Khaliullin, T. Ku´s, A. Landau, J. Liu, E. I. Proynov, Y. M. Rhee, R. M. Richard, M. A. Rohrdanz, R. P. Steele, E. J. Sundstrom, H. L. Woodcock, P. M. Zimmerman, D. Zuev, B. Albrecht, E. Alguire, B. Austin, G. J. O. Beran, Y. A. Bernard, E. Berquist, K. Brandhorst, K. B. Bravaya, S. T. Brown, D. Casanova, C.-M. Chang, Y. Chen, S. H. Chien, K. D. Closser, D. L. Crittenden, M. Diedenhofen, R. A.

DiStasio, H. Do, A. D. Dutoi, R. G. Edgar, S. Fatehi, L. Fusti-Molnar, A. Ghysels, A. Golubeva-Zadorozhnaya, J. Gomes, M. W. Hanson-Heine, P. H. Harbach, A. W. Hauser, E. G. Hohenstein, Z. C. Holden, T.-C. Jagau, H. Ji, B. Kaduk, K. Khistyaev, J. Kim, J. Kim, R. A. King, P. Klunzinger, D. Kosenkov, T. Kowalczyk, C. M. Krauter, K. U. Lao, A. D. Laurent, K. V. Lawler, S. V. Levchenko, C. Y. Lin, F. Liu, E. Livshits, R. C. Lochan, A. Luenser, P. Manohar, S. F. Manzer, S.-P. Mao, N. Mardirossian, A. V. Marenich, S. A. Maurer, N. J. Mayhall, E. Neuscamman, C. M. Oana, R. Olivares-Amaya, D. P. O'Neill, J. A. Parkhill, T. M. Perrine, R. Peverati, A. Prociuk, D. R. Rehn, E. Rosta, N. J. Russ, S. M. Sharada, S. Sharma, D. W. Small, A. Sodt, T. Stein, D. St¨uck, Y.-C. Su, A. J. Thom, T. Tsuchimochi, V. Vanovschi, L. Vogt, O. Vydrov, T. Wang, M. A. Watson, J. Wenzel, A. White, C. F. Williams, J. Yang, S. Yeganeh, S. R. Yost, Z.-Q. You, I. Y. Zhang, X. Zhang, Y. Zhao, B. R. Brooks, G. K. Chan, D. M. Chipman, C. J. Cramer, W. A. Goddard, M. S. Gordon, W. J. Hehre, A. Klamt, H. F. Schaefer, M. W. Schmidt, C. D. Sherrill, D. G. Truhlar, A. Warshel, X. Xu, A. Aspuru-Guzik, R. Baer, A. T. Bell, N. A. Besley, J.-D. Chai, A. Dreuw, B. D. Dunietz, T. R. Furlani, S. R. Gwaltney, C.-P. Hsu, Y. Jung, J. Kong, D. S. Lambrecht, W. Liang, C. Ochsenfeld, V. A. Rassolov, L. V. Slipchenko, J. E. Subotnik, T. Van Voorhis, J. M. Herbert, A. I. Krylov, P. M. Gill and M. Head-Gordon, *Mol. Phys.*, 2015, **113**, 184–21.

8. S. Grimme, J. Antony, S. Ehrlich and H. Krieg, *J. Chem. Phys.*, 2010, **132**, 154104.

9. V. N. Staroverov, G. E. Scuseria, J. Tao and J. P. Perdew, *J. Chem. Phys.*, 2003, **119**, 12129–12137.

10. F. Weigend and R. Ahlrichs, *Phys. Chem. Chem. Phys.*, 2005, **7**, 3297–3305.

11. A. Behn, P. M. Zimmerman, A. T. Bell and M. Head-Gordon, *J. Chem. Phys.*, 2011, **135**, 224108.

12. S. Mallikarjun Sharada, P. M. Zimmerman, A. T. Bell and M. Head-Gordon, *J. Chem. Theory Comput.*, 2012, **8**, 5166–5174.

13. E. D. Glendening, C. R. Landis and F. Weinhold. *Wiley Interdiscip. Rev.: Comput. Mol. Sci.*, 2012, **2**, 1–42.